Group-velocity-mismatch-induced transition from absolute to convective instability in birefringent fibers

L. Drouzi,[1,2] S. Coulibaly,[1] M. Taki,[1] and K. Laabidi[2]
[1]*Université de Lille, CNRS, UMR 8523 - PhLAM - Physique des Lasers Atomes et Molécules, F-59000 Lille, France*
[2]*Université Mohamed Premier - LDOM - Laboratoire de Dynamique et d'Optique des Matériaux, Oujda, Maroc*
(Received 27 March 2017; published 19 June 2017)

In nonlinear fiber systems operating in pulsed regime, the pumping excitation is no longer time extended (cw regime) but localized in time with a finite duration. In this case, standard linear stability analysis (often called modulational instability), as it stands, fails to describe the linear time evolution inside the fiber and one has to reformulate the problem as an initial value problem leading to convective and absolute instabilities. We show, in normal dispersion regime, that the dynamical evolution of a localized probe in a highly birefringent optical fiber results in a modulational instability splitting into convective and absolute instabilities. We have also characterized the splitting in terms of coupling of the group-velocity mismatch between the two polarized states and the total injected pump power. We evidenced a transition from absolute to convective regime and characterized the qualitative difference of the dynamics in the two regimes. The results of the numerical integration of the governing equations are in excellent agreement with our analytical findings and may contribute to understanding the complex dynamics appearing in the time domain of the supercontinuum generation that plays a key role in the formation of optical rogue waves.

DOI: 10.1103/PhysRevA.95.063826

I. INTRODUCTION

Modulational instability (MI) is the process by which a periodic state rises spontaneously from a homogeneous state. This process was first reported more than 40 years ago [1,2], and observed in numerous physical systems, including hydrodynamics [3], plasma physics [4,5], nonlinear optics [6,7], and Bose-Einstein condensation [8], just to cite a few. Despite this long and important history, MI keeps attracting a great interest from both a fundamental and a technological point of view, particularly in nonlinear optics. Indeed, MI has been identified to play a crucial role in the dynamics of rogue wave [9,10] and supercontinuum (SC) generation [11].

Theoretically, MI mainly provides two quantities: the growth rate—gain—and the periodicity—wave number or pulsation. Gain and periodicity of the MI are obtained by the standard linear stability analysis. In this analysis, the solutions of the linearized equations of the system are assumed to have a monochromatic wave form [12,13]. It is clear that this analysis is convenient for instabilities seeded by extended fluctuations, e.g., noise. Indeed, when the instability is seeded by a localized perturbation, one has to characterize the growth of this disturbance in both space and time. Therefore, the use of the spatiotemporal theory in terms of convective and absolute instability must be employed. Developed since the early 1950s [14–16], this theory attempts to address the answer to the following questions. How does one describe the dynamical evolution of a localized pulse (wave packet) with both finite duration and size (finite spectrum and finite wave number) that emerges from fluctuations in unstable regime? What are the career frequency und wave number of the merging pulse? And more importantly what is the group velocity of the pulse? In the course of its evolution, does it spread in all directions (absolute unstable regime) or not (convective unstable regime)? And, if any, is there any transition from one regime to another? The answers to these questions are even more fundamental when the considered system exhibits a breaking of parity symmetry (for fiber systems it is a time-reversal symmetry).

In the context of fiber optics, symmetry-breaking terms have been shown to introduce a rich variety of phenomena [17–22]. Examples include the harnessing of rogue wave generation by the slope of the fiber dispersion curve and soliton explosion under effects of the noninstantaneous response of the fused-silica Raman effect [11,23]. In these aforementioned examples, the symmetry breaking is coming from modal effects due to the wave form of the light propagating in the fiber. However, symmetry breaking can also be induced geometrically when designing the fiber. In such a fiber, the built-in birefringence can be made much larger than random birefringence variation. Hence the vectorial nature of wave propagation must be considered. In this case, the copropagating orthogonally polarized fields are found to exhibit the MI in both cases of normal and anomalous group-velocity dispersion (GVD) [24–27], in contrast to scalar fibers where the MI takes place only in anomalous GVD region. In terms of convective and absolute instability, it is also known that the nonlinear Schrödinger (NLS) equation that describes the spatiotemporal dynamics of the wave envelope along the fiber does not display a transition from one regime to another. The same situation is encountered in weak birefringence regime while considering the vectorial NLS equations. We emphasize here that the existence of this transition is identified in the high birefringence fiber systems.

In this paper we consider the dynamical evolution of a localized probe in a highly birefringent optical fiber by means of absolute and convective instabilities theory. We were able to single out the existence of a transition between the two regimes. The latter results from the splitting of MI into absolute and convective ones. The dynamics and the evolution of the solutions are drastically different in the two regimes. More precisely, in a convectively unstable regime, the system is strongly sensitive to noise sources and exhibits

propagating noise-sustained solutions whereas, in absolutely unstable regime, the dynamics is dominated by nonlinear dynamical solutions. We have characterized the splitting, in terms of nonlinear birefringent coupling, the group-velocity mismatch between the two polarized states and the total injected pump power. The results of the numerical integration of the governing equations are in excellent agreement with our analytical findings.

The paper is organized as follows. In Sec. II we give the governing equations describing the evolution of a highly birefringent optical fiber including nonlinear birefringent coupling and the group-velocity mismatch between the two polarized states of light propagating along the fiber. Standard modulational stability is recalled with a new emphasis on the role of the nonlinear birefringent coupling term in the characteristics and thresholds of instabilities. In Sec. III we analyze the response of the highly birefringent fiber to an impulse perturbation by means of absolute and convective instabilities analysis. The significant role of the group velocity of the unstable emerging wave packet (or pulse) in the nature of the instability is emphasized. Section IV is devoted to both analytical and numerical demonstration of the existence and the characterization of the transition between absolute and convective instability and the dynamics of the solutions in these regimes. Numerical solutions obtained by integrating the governing equations of a highly birefringent fiber are in excellent agreement with our predictions. Concluding remarks are contained in the last section.

II. MODEL AND MODULATIONAL INSTABILITY ANALYSIS

Let's start with the coupled generalized NLS equations satisfied by the orthogonally polarized components of a pulse in a lossless and a highly birefringent optical fiber:

$$\frac{\partial A_x}{\partial Z} = -i\frac{\beta_2}{2}\frac{\partial^2 A_x}{\partial t^2} + i\gamma(|A_x|^2 + B|A_y|^2)A_x, \tag{1a}$$

$$\frac{\partial A_y}{\partial Z} = -i\frac{\beta_2}{2}\frac{\partial^2 A_y}{\partial t^2} - 2b_0\frac{\partial A_y}{\partial t} + i\gamma(|A_y|^2 + B|A_x|^2)A_y, \tag{1b}$$

where $A_x(Z,t)$ and $A_y(Z,t)$ stand for the two orthogonal components of an arbitrary polarized optical field $\mathbf{E}(z,t)$ at the carrier frequency ω_0, i.e.,

$$\mathbf{E}(z,t) = \tfrac{1}{2}[A_x(z,t)\hat{x} + A_y(z,t)\hat{y}]e^{i(\beta_0 z - \omega_0 t)} + \text{c.c.},$$

where $\beta_0 = (\beta_{0x} + \beta_{0y})/2$ is the average propagation constant. β_2, B, and γ are the GVD, nonlinear birefringent coupling (or cross phase modulation) and Kerr nonlinearity parameters, respectively [27]. Here we have set the moving frame variable $Z = z + t/\beta_{1x}$ associated to the $\hat{x}$ axis. $b_0 = (\beta_{1y} - \beta_{1x})/2$ accounts for the group-velocity mismatch between the two polarization states.

Equations (1) have a continuous-wave (cw) solution which reads $A_j = A_{j0}\exp(i\phi_j z)$, where $\phi_j = \gamma(|A_{j0}|^2 + B|A_{j'0}|^2)$ with $(j,j') = (x,y)$ and (y,x) for the x axis and y axis, respectively. The standard stability analysis of this solution against *monochromatic* perturbations of the form $e^{i(\omega t - kz)}$ leads to the following dispersion relation:

$$\mathcal{D}(k,\omega) = [(k - 2b(\omega))^2 - H(\omega)][k^2 - H(\omega)] - C(\omega)^2 = 0, \tag{2}$$

with k being the wave number and ω the pulsation. In this relation, $H(\omega) = \beta_2\omega^2(\beta_2\omega^2/4 + \gamma P)$, $C(\omega) = B\beta_2\gamma P\omega^2$, and $b(\omega) = b_0\omega$, where we have set $|A_{x0}|^2 = |A_{y0}|^2 = P$, the pump power on each polarization state. Next, linear stability analysis allows one to determine when the wave number k possesses an imaginary part for some real values of the pulsation ω. Hence the cw is said unstable (stable) if $k_i = \text{Im}(k)$ is positive (negative). In addition to this stability condition, one may be interested in the most amplified frequency and the associated gain if an instability band of frequency exists. Hence it is obvious that this most amplified frequency is obtained by solving the following equation:

$$\left.\frac{\partial k_i}{\partial \omega}\right|_{\omega_c} = 0,$$

such that $\partial^2_\omega k_i|_{\omega_c} < 0$, and the maximum gain spectrum is given by $g = 2k_i(\omega_c)$. From linear stability analysis, cumbersome but straightforward calculations lead to the instability frequency bands that are delimited by the following four frequencies:

$$\omega_1^{\pm} = \pm 2\sqrt{(B-1)\beta_2\gamma P + b_0^2}/\beta_2, \tag{3a}$$

$$\omega_2^{\pm} = \pm 2\sqrt{-(1+B)\beta_2\gamma P + b_0^2}/\beta_2. \tag{3b}$$

We focus here in the normal dispersion regime. In this case, an examination of these expressions shows the crucial role of the nonlinear birefringent parameter B in the dynamics. First, let's recall that B depends on the type of polarization and varies from $B = 2/3$ to $B = 2$ [27]. We have summarized in Fig. 1 the results of the linear stability analysis as a function of B. For $B \geqslant 1$, it can be seen from Fig. 1 that MI exists for any power pump value leading to two symmetrical unstable sidebands connected to the zero frequency and limited by the frequencies $\omega_1^{\pm}$. By decreasing the pump power a transition is reached at $P = P_t = b_0^2/(\beta_2\gamma(1+B))$ [see zone (4) in Fig. 1] where two

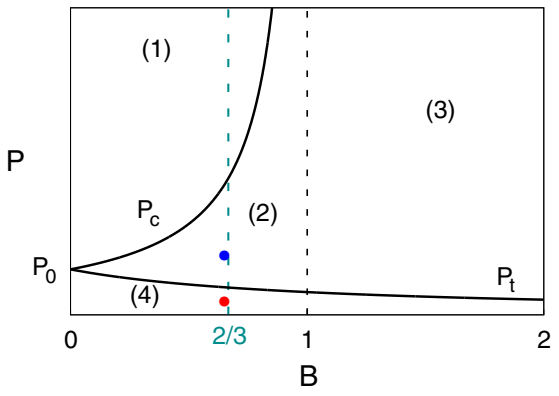

FIG. 1. Curve P_c is the instability threshold and P_t is the transition curve from two to four limiting sidebands frequencies as functions of B. Their expressions are defined in the text. The parameters are $\beta_2 = 0.06\ \text{ps}^2\,\text{m}^{-1}$, $b_0 = 0.2\ \text{ps}\,\text{m}^{-1}$, and $\gamma = 15\ \text{W}\,\text{km}^{-1}$.

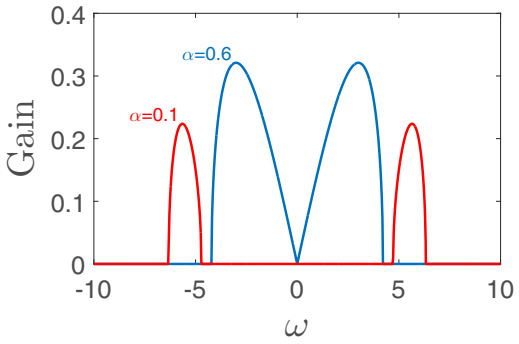

FIG. 2. Typical vector modulational instability gain curve profiles. Power gain $[G = 2\,\mathrm{Im}(k)]$ with $\beta_2 = 0.06\ \mathrm{ps^2\,m^{-1}}$, $b_0 = 0.2\ \mathrm{ps\,m^{-1}}$, $\gamma = 15\ \mathrm{W\,km^{-1}}$, and $B = 2/3$. $\alpha = P/P_c$, where P_c is the critical power threshold of instability defined in the text.

new frequencies $\omega_2^{\pm}$ are generated giving rise to two separated lobes of instability. On the other hand, when $B < 1$, the case we are interested with, MI only exists below a critical pump power $P_c = b_0^2/[\beta_2\gamma(1-B)]$ [see zones (1) and (2) in Fig. 1]. Note that this result has already been observed in highly birefringent optical fibers [24,27]. In this case and for more convenience, we introduce $\alpha = P/P_c$ as a ratio between the pump power and the critical power P_c, which will be used as a control parameter. Hence the instability bands are well separated if $P < P_t$ [zones (4) in Fig. 1] and continuous otherwise [zones (2) on Fig. 1]. In what follows, we set $B = 2/3$ and show in Fig. 2 a typical example of two instability lobes on both sides of P_t as indicated by the two solid circles in Fig. 1. Finally, note that when $B = 1$, this is a particular and interesting case when Eqs. (1) reduce to an integrable coupled nonlinear Schrödinger system known as the Manakov system [28] and can be solved with the inverse scattering transform method (IST). By contrast to the classical linear stability described above, when the evolution of the system is initiated by a localized perturbation, it is necessary to include a finite band of modes in the dynamical description. This can be achieved by reformulating the linear stability analysis as an initial-value problem. This makes possible determining the main dynamical characteristics of the wave packet on the basic state including growth rate, instantaneous frequency, wave number, and, more importantly, its velocity as we will show in the following.

III. CONVECTIVE AND ABSOLUTE INSTABILITY

Developed by Briggs [29], the study of the dynamics of localized linear disturbances, i.e., absolute and convective instabilities, of a given base solution is treated as a linear initial-value problem. The key tool consists of the evaluation of the asymptotic solution of the problem in both space and time, using a combined Fourier-Laplace transform and a consistent mathematical formalism (see also [30]). This theory has been recently revisited in the framework of the scalar NLS [31] and will not be detailed in this work.

Note that an important study of the nonlinear stage of the modulation instability, in a scalar focusing (anomalous dispersion) nonlinear Schrödinger equation, has been performed in [32] where a new class of solitonic (nonlinear) solutions, which can be generated from localized perturbations, has been found. Later on, some of these solitonic solutions have been experimentally evidenced in both water waves and optics [33]. Here, in contrast, we concentrate, in the normal dispersion regime, on the impact of time-reversal symmetry breaking introduced by the birefringence (group-velocity mismatch) on the MI splitting into convective and absolute ones and the evolution of localized perturbations of the cw stationary solutions. The link between our localized solutions and the solutions generated from localized perturbations in the strongly nonlinear regime is out of the scope of this paper.

The main purpose here is to describe the dynamical behavior of asymptotical solutions and their properties. Following the method developed in [31], the solution can be evaluated by the following Fourier-Laplace integrals:

$$A_j(z,t) = \int_{-\infty}^{\infty} d\omega \int_{i\sigma-\infty}^{i\sigma+\infty} \frac{S_j(\omega,k)}{\mathcal{D}(\omega,k)} e^{i(\omega t - kz)} dk, \qquad (4)$$

where $S_j(\omega,k)$ and $A_j(z,t)$, with $j = x$ or y, represent the Fourier transform of the initial conditions and the solution of the linear problem, respectively. $\mathcal{D}(\omega,k)$ is the dispersion-relation function (2). Here σ in the Laplace integral is assumed greater than the maximum growth rate of any monochromatic wave (for more details, see [31]).

In principle, the asymptotic behavior of integral (4) can be evaluated using the steepest descent method in the framework of the saddle-point approach [34]. However, it has been demonstrated that the existence of a saddle point does not guarantee the existence of a growing perturbation [35]. Indeed, only the collision criterion—pinching condition—allows the identification of the contributing saddle point. Hence, for a contributing saddle point, tuning σ from $+\infty$ to $-\infty$, at least two ω roots of the dispersion relation have to originate from opposite sides of the complex plane and move towards each other, collide at a specific point, then move in the opposite direction. At this specific pinching point, ω and k have to hold the following conditions:

$$\mathcal{D}(\omega, k+\omega V) = 0, \quad \frac{\partial \mathcal{D}(\omega, k+\omega V)}{\partial \omega} = 0, \qquad (5)$$

where V is the velocity of the frame in which the integral is evaluated, which corresponds here to the wave packet group velocity (retarded time frame). Therefore, the transition between convective and absolute instability is studied in the laboratory frame, i.e., for $V = 0$. Indeed, in the convective regime, only saddle points with the same sign of velocities (pulses propagating in the same direction) contribute to the instability, while in the absolute regime the saddle points that contribute to the instability are those with both positive and negative velocities (pulses propagating in the opposite directions). In order to get more insight about the transition, let us set V_+ the velocity of the leading front (the fastest one) of the pulse and V_- that of rear limiting front (the slowest one) of the pulse. Therefore, the absolute and convective regimes are characterized by $V_+V_- < 0$ (the spreading of the pulse) and $V_+V_- > 0$ (pulse propagating in one direction without spreading), respectively [36].

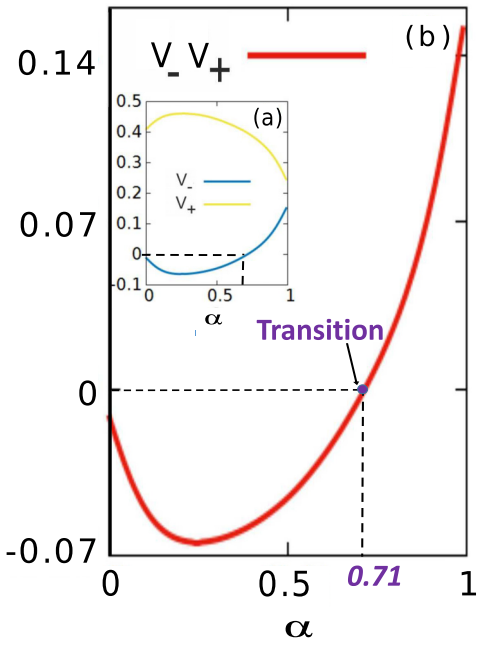

FIG. 3. (a) Inset gives the separate evolution of the V_+ (yellow) and V_- blue. (b) Evolution of the product V_-V_+ vs the normalized power control parameter α showing the transition point $\alpha_t = 0.71$ corresponding to $V_-V_+ = 0$. The parameters are $\beta_2 = 0.06\ \mathrm{ps^2\,m^{-1}}$, $b_0 = 0.2\ \mathrm{ps\,m^{-1}}$, $B = 2/3$, and $\gamma = 6\ \mathrm{W\,km^{-1}}$.

IV. RESULTS

We start by checking the possibility of a transition between absolute and convective instability through the dispersion relation (2). For this purpose, we need to explicitly determine the velocities $V_\pm$, mentioned above, by solving the following system of equations:

$$\frac{\partial k}{\partial \omega} = V_\pm, \tag{6}$$

$$\frac{\partial^2 k}{\partial \omega^2} = 0. \tag{7}$$

By substituting $k(\omega)$ from (2) into the above equations and after cumbersome but straightforward calculations, we end up with an intractable polynomial equation in k and ω, which is of twelfth (third) degree in ω (k). We have numerically solved these polynomial equations in order to determine and follow the product V_+V_- with respect to the total pump power P. The result of this resolution is summarized in Fig. 3 where we have plotted the product V_+V_- as a function of the control parameter $\alpha = P/P_c$ introduced in Sec. II. As can be seen from this figure, for a set of parameters, the transition from convective to absolute instability is reached for a value of the control parameter $\alpha_t \simeq 0.71$ when the product V_+V_- vanishes. The transition point is indicated on the figure and the inset displays the leading and the rear front velocities V_+ and V_-, respectively, and shows the lowest velocity V_- crossing zero, which means that the necessary condition for the instability transition holds. For the instability to actually occur in the system the corresponding saddle point must verify the pinching sufficient condition. Indeed, in the absolute regime the saddle point should contribute to the instability with a positive gain, while in the convective case it should contribute with a negative or at best a zero gain. To demonstrate the existence of the transition, to illustrate the dynamics of its emergence, and to show how the pinching condition gives rise to the instability, we have displayed the evolution in complex planes of the wave numbers k and the frequencies ω in Figs. 4, 5, and 6 for three typical values of the control parameter α. Note that it is not surprising that both the wave number and the frequency are complex since Re(k) [Re(ω)] accounts for the wave number (the frequency), whereas Im(k) [Im(ω)] corresponds to the gain (the temporal decay) of the pulse.

First, let us focus on Fig. 4 where we have numerically solved the dispersion relation (2) for the control parameter $\alpha = 0.2$ in the absolute regime (see Fig. 3). The left panel gives the k path and the right one represents the trajectory in the ω branches. In this figure, K_r (ω_r) and K_i (ω_i) stand for the real and imaginary parts of the saddle-point wave number (frequency), respectively. We have adopted the following numerical approach. First, we fix $K_r = K_{sr}$, $K_{r-} = K_{sr} - 0.01$, and $K_{r+} = K_{sr} + 0.01$ and second we vary, for the three cases, K_i in an appropriate range around K_{si},

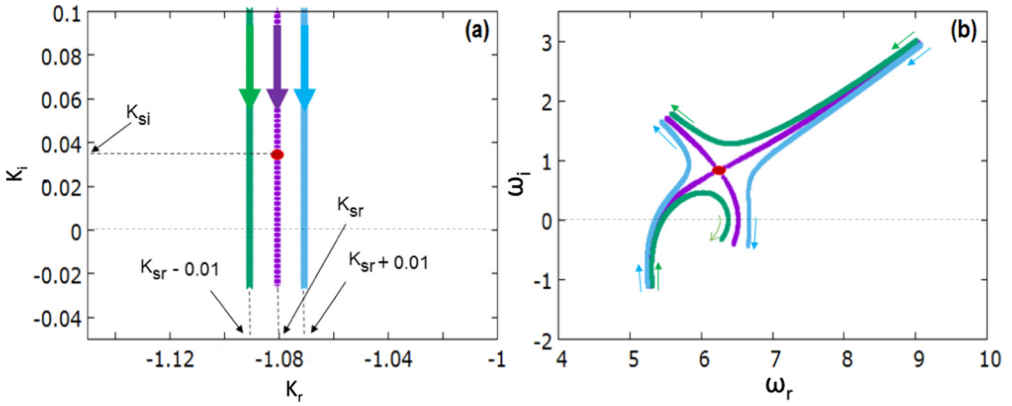

FIG. 4. Illustration of pinching condition in the case of absolute instability regime. (a) Paths in the complex plane (k_r,k_i) and (b) the corresponding trajectories in the complex plane (ω_r,ω_i) around the computed saddle point $k_s = -1.08 + 0.04i$. The same parameters as in Fig. 3 with $\alpha = 0.2$.

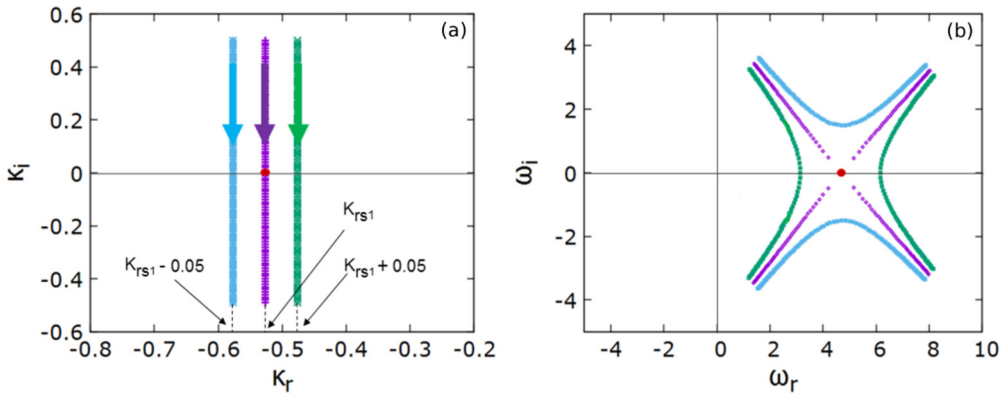

FIG. 5. Illustration of pinching condition in the case of convective instability regime. (a) Paths in the complex plane (K_r, K_i) and (b) the corresponding trajectories in the complex plane (ω_r, ω_i). Note the computed real part of the saddle point $K_{sr} = -0.52$. The same parameters as in Fig. 3 and $\alpha = 0.9$.

which is the growth rate of instability. For $K_{r-} = K_{sr} - 0.01$ fixed and by decreasing K_i, the complex K plane shows a vertical line (extreme left one) as it should be. As can be seen from the right panel, two ω branches appear from both sides of the complex ω plane (green curves) and their evolution is indicated by the arrows. By fixing $K_{r+} = K_{sr} + 0.01$, one observes, in the complex ω plane, two new ω–branches (blue curves) associated with the blue vertical line but with a different structure. Finally, for $K_r = K_{sr}$ (central line), the two ω branches collide giving rise to the saddle point indicated by a red circle in the figure. The most important is the whole dynamics around the emergence of the saddle point that we summarize as follows: the green and blue paths in Fig. 4 show the trajectories before and after the saddle point, respectively. By varying K, two ω branches appearing from both sides of complex ω (green curves) collide at the saddle point (red curves) and separate after collision (blue curves). The important result is that when the collision occurs in the ω plane the imaginary part of the corresponding saddle point K_{si} is positive, leading to an actual absolute instability. It is worthy to note that the main difficulty to detect the absolute and convective nature of the instability remains in the fact that not all saddle points satisfy the pinching condition (or the Bers collision criteria). One may refer to [35] where several examples of saddle points not verifying the pinching condition and, more importantly, do not lead to any instability are reported. The same approach has been applied to produce the results in Fig. 5 where the control parameter was fixed to $\alpha = 0.9$ to account for the convective instability. As can be seen from this figure, the ω-branch structures are less complex. But the significant result remains in the imaginary part of the saddle point, which is now null showing that the instability is not absolute but convective. It is worthy to note that, for these values of parameters, the system is modulationally unstable. The transition between the two regimes is displayed in Fig. 6 where we have set $\alpha = \alpha_t = 0.71$. The collision of two saddle points is clearly shown, which is the signature of a such transition [36]. This is a critical situation characterizing the complex behavior that may be exhibited in conservative systems. This transition is detected in fiber systems and it is mainly the consequence of the group-velocity mismatch between the two polarization states. Moreover, the nonlinear birefringence coefficient B may have a crucial role in the dynamics of the instabilities since it may drastically impact the transition between convective and absolute instabilities and the characteristics (wave number, frequency, and velocity) of the emerging solutions.

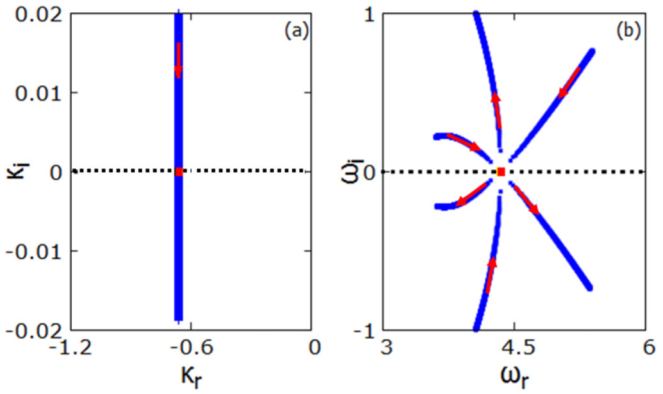

FIG. 6. Illustration of pinching condition at transition point $\alpha_t = 0.71$ between absolute and convective instability. (a) Paths in the complex plane (k_r, k_i) and (b) the corresponding trajectories in the complex plane (ω_r, ω_i). Note the presence of three branches showing the collision of two saddle points. The parameters are the same as in Fig. 3.

Therefore, we are able to conclude that highly birefringent fiber systems can exhibit an absolute and convective instability transition. Moreover, our analytical predictions are in excellent agreement with the solutions obtained from the numerical integration of the master equations (1). The results are depicted in Fig. 7, where we have fixed the control parameter to $\alpha = 0.4$, 0.9, and 0.71 to show the emerging solutions in absolute and convective regimes together with the transition between them, respectively. This figure displays the spatiotemporal maps of the intensity (bottom panel) together with the spatiotemporal gain (top panels) with respect to the propagation velocity. The spatiotemporal (or global) gain is the most significant gain that takes into account not only the standard growth rate (K_i, as may be obtained by MI) but it also includes the propagative character that is crucial in the instability of the pulse. We emphasize here that as far

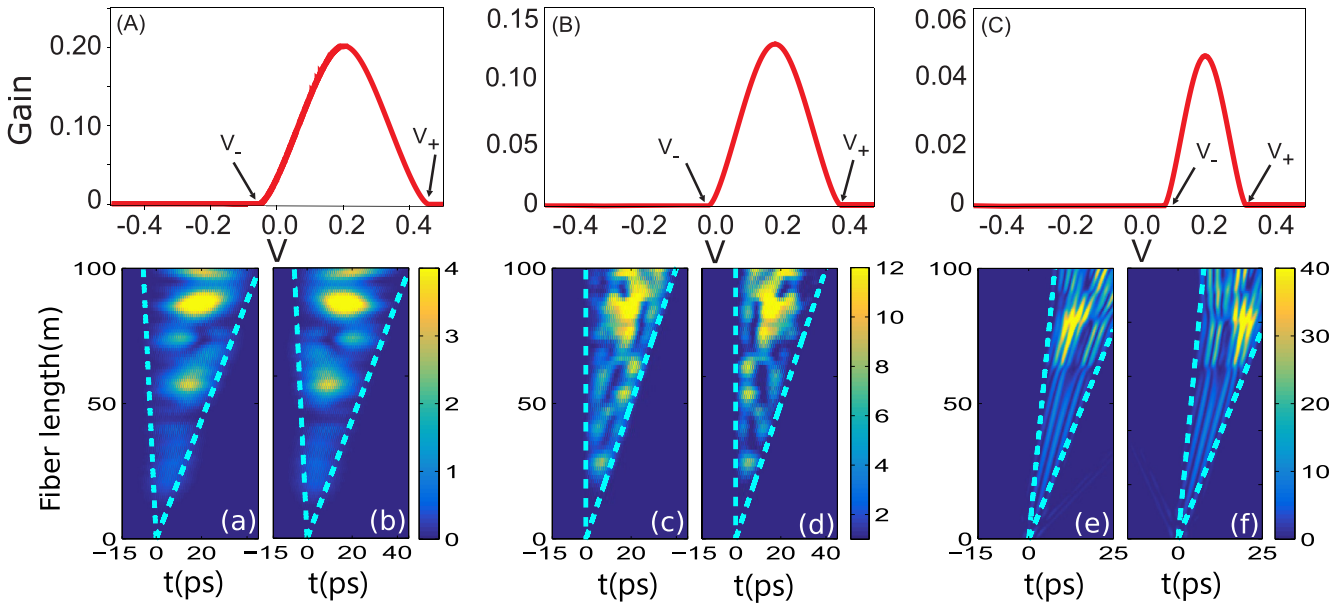

FIG. 7. Spatiotemporal evolutions (bottom panel) of the numerically computed intensities along the neutral axes of the birefringent fiber for $\alpha = 0.4$ [(a),(b)], 0.71 [(c),(d)], and 0.9 [(e),(f)]. Dash lines represent the limit of the wave packet. The top panel gives the gain profile with respect to the velocity of an observer moving with the velocity V. The other parameters are the same as in Fig. 3.

as monochromatic (plane) waves are concerned the growth rate K_i is pertinent but fails to describe the instability to localized perturbations. As can be seen in Fig. 7 (top panels) there are two specific velocities denoted V_- and V_+ where the global gain vanishes. These two velocities that are indicated by dashed lines in the spatiotemporal maps (bottom panels), delimit the cone of unstable solutions. We can observe in the figure that the instability spreads with positive and negative velocities in the absolute regime [Figs. 7(A), 7(a), and 7(b)], only with a zero and a positive velocity at the transition [Figs. 7(B), 7(c), and 7(d)] and with two positive velocities in the convective regime [Figs. 7(C), 7(e), and 7(f)]. Note that the maximum gain is drastically reduced after the transition when $\alpha = 0.9$ since this value of α is close to the extinction of the instability ($\alpha = 1$). Since the transition is sensitive to the values of both the normalized injected power α and the nonlinear birefringence parameter B, we have plotted the maximum gain with respect to α and B in Fig. 8 and Fig. 9, respectively. As can be seen from Fig. 8, the transition point lies in the descendent part of the curve, which confirms the gain reduction after the transition. Interestingly, Fig. 9 shows that the maximum gain increases with increasing B. A striking feature appears at transition when $V_- = 0$. Indeed, this case corresponds to zero global gain but according to the steepest descent method, the asymptotic behavior of any perturbation follows the $1/\sqrt{Z}$ scaling law. This statement is confirmed by the numerical integration of the master equations

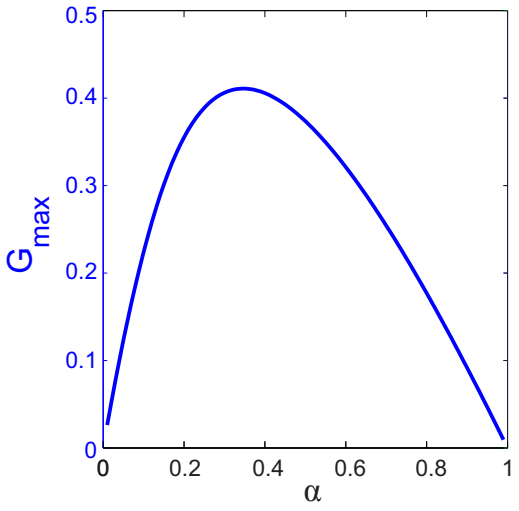

FIG. 8. Maximum gain vs the parameter α for $B = 2/3$. Note that the transition point $\alpha = 0.71$ lies in the descendent part of the curve. The parameters are $\beta_2 = 0.06$ ps^2 m^{-1}, $b_0 = 0.2$ ps m^{-1}, and $\gamma = 6$ W km^{-1}.

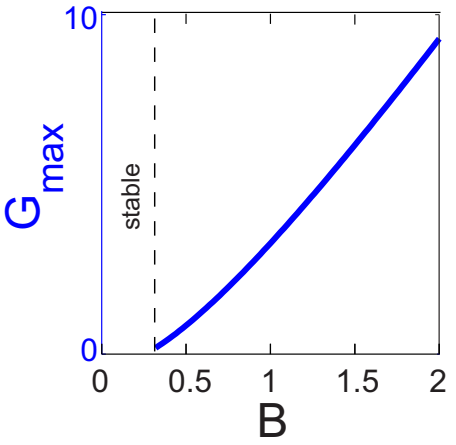

FIG. 9. Maximum gain vs the parameter B. Note that the maximum gain increases with increasing B. The parameters are $\beta_2 = 0.06$ ps^2 m^{-1}, $b_0 = 0.4$ ps m^{-1}, and $\gamma = 6$ W km^{-1}.

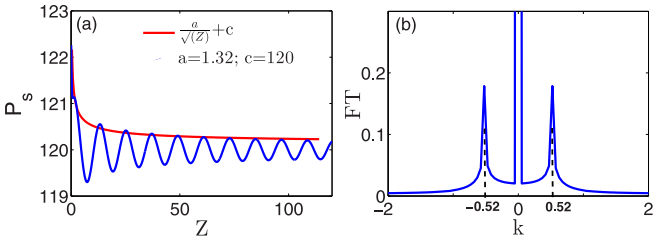

FIG. 10. (a) Evolution of the intensity vs the propagation length Z at the location ($t = 0$) of initial localized perturbation (blue solid line). The red dash line corresponds to the result of the fit of the envelop with varying as $c + \frac{1}{\sqrt{Z}}$. The The other parameters are the same as in Fig. 3 with $\alpha = 0.9$. (b) Fourier spectrum of the evolution given in (a).

(1) where we have recorded the intensity of the field along the x axis [solid line of Fig. 10(a)]. The evolution confirms the decay of the intensity and the envelope evolution fits as $a/\sqrt{Z} + b$ showing a good agreement with the analytical results. In addition, the wave number corresponding to the oscillations of the intensity is also in good agreement with our analytical predictions as can be seen from Fig. 10(b), where we have plotted the Fourier spectrum of the aforementioned record. This contrasts with the marginal (gain = 0) instability in the standard MI where a monochromatic wave persists asymptotically since it is neither attenuated nor amplified. This apparent contrast can be explained as a standard result when applying the steepest method to find the asymptotic stable propagating waves in dispersive media. Modulation instability as it stands fails to predict this asymptotic wave behavior since it concerns monochromatic waves and, by the way, ignores the propagation character of dispersive waves, which needs to reformulate the instability problem as an initial-value problem.

V. CONCLUSION

In conclusion, we have shown that in the highly birefringent fiber systems and in the normal dispersion regime, a transition between convective and absolute unstable regimes exists. This transition has been described by means of a control parameter that measures the distance from the extinction of all the instabilities in the system. Our analytical approach allows, in terms of convective and absolute instabilities, determining the main dynamical characteristics of the propagating pulse in a form of a wave packet. This includes growth rate, instantaneous frequency, wave number, and, more importantly, its total group velocity resulting from both the mismatch and the coupling between the two polarized states. Our findings are in excellent agreement with numerical solutions obtained by integrating the governing equations. The results are not specific to nonlinear fiber systems since time-reversal or reflection symmetry breaking (in spatially extended systems) are present in such diverse fields as plasma physics, hydrodynamics, and reaction diffusion systems. We thus believe that the results obtained here can be of interest for a wide range of physical areas. Further analysis of the nonlinear interaction between the pulses together with the different dynamics occurring in absolute and convective regimes is in progress.

ACKNOWLEDGMENTS

The authors acknowledge the support of the "Laboratoire d'Excellence CEMPI: Centre Européen pour les Mathématiques, la Physique et leurs Interactions" (Grant No. ANR-11-LABX-0007-01). This research was supported in part by the Interuniversity Attraction Poles program of the Belgium Science Policy Office under Grant No. IAP P7-35 «photonics@be», the French Agence Nationale de la Recherche project OptiRoc No. ANR-12-BS04-0011, and by the CPER Photonics for Society.

[1] T. B. Benjamin and J. E. Feir, J. Fluid Mech. **27**, 417 (1967).
[2] V. I. Bespalov and V. I. Talanov, Zh. Eksp. Teor. Fiz., Pis'ma Red. **3**, 471 (1966) [JETP Lett. **3**, 307 (1966)].
[3] C. Kharif and E. Pelinovsky, Eur. J. Mech. B Fluids **22**, 603 (2003).
[4] C. N. Lashmore-Davies, D. R. McCarthy, and A. Thyagaraja, Phys. Plasmas **8**, 5121 (2001).
[5] T. Taniuti and H. Washimi, Phys. Rev. Lett. **21**, 209 (1968).
[6] K. Tai, A. Hasegawa, and A. Tomita, Phys. Rev. Lett. **56**, 135 (1986).
[7] G. P. Agrawal, Phys. Rev. Lett. **59**, 880 (1987).
[8] V. V. Konotop and M. Salerno, Phys. Rev. A **65**, 021602(R) (2002).
[9] M. Taki, A. Mussot, A. Kudlinski, E. Louvergneaux, M. Kolobov, and M. Douay, Phys. Lett. A **374**, 691 (2010).
[10] D. R. Solli, C. Ropers, P. Koonath, and B. Jalali, Nature (London) **450**, 1054 (2007).
[11] J. M. Dudley, G. Genty, and S. Coen, Rev. Mod. Phys. **78**, 1135 (2008).
[12] P. G. Drazin and W. H. Reid, *Hydrodynamic Stability* (Cambridge University Press, Cambridge, UK, 2004).
[13] S. Chandrasekhar, *Hydrodynamic and Hydromagnetic Stability* (Dover, New York, 1981).
[14] L. D. Landau and E. M. Lifshitz, *Electrodynamics of Continuous Media* (GITTL, Moscow, 1953).
[15] R. Q. Twiss, Proc. Phys. Soc. London, B **64**, 654 (1951).
[16] E. J. Greer, D. M. Patrick, P. G. Wigley, and J. R. Taylor, Electron. Lett. **25**, 1246 (1989).
[17] A. Demircan, M. Pietrzyk, and U. Bandelow, Opt. Quantum Electron. **40**, 455 (2008).
[18] A. Mussot, A. Kudlinski, E. Louvergneaux, M. Kolobov, and M. Taki, Opt. Lett. **35**, 1194 (2010).
[19] N. Akhmediev, A. Ankiewicz, J. M. Soto-Crespo, and J. M. Dudley, Phys. Lett. A **375**, 775 (2011).
[20] A. Mussot, A. Kudlinski, M. Droques, P. Szriftgiser, and N. Akhmediev, Phys. Rev. X **4**, 011054 (2014).
[21] G. Weerasekara, A. Tokunaga, H. Terauchi, M. Eberhard, and A. Maruta, Opt. Express **23**, 143 (2015).
[22] S. Coulibaly, Z. Liu, M. Taki, and G. P. Agrawal, Phys. Rev. A **86**, 033802 (2012).

[23] A. Mussot, A. Kudlinski, M. Kolobov, E. Louvergneaux, M. Douay, and M. Taki, Opt. Express **17**, 17010 (2009).
[24] J. E. Rothenberg, Phys. Rev. A **42**, 682(R) (1990).
[25] S. Wabnitz, Phys. Rev. A **38**, 2018 (1988).
[26] G. Millot, E. Seve, S. Wabnitz, and M. Haelterman, J. Opt. Soc. Am. B **15**, 1266 (1998).
[27] G. P. Agrawal, *Nonlinear Fiber Optics*, 5th ed. (Academic Press, New York, 2013).
[28] S. V. Manakov, Sov. Phys. JETP **38**, 248 (1974).
[29] R. J. Briggs, *Electron-stream Interaction with Plasmas* (MIT Press, Cambridge, MA, 1964).
[30] A. Bers, in *International Congress on Waves and Instabilities in Plasmas*, edited by G. Auer and F. Cap (Institute for Theoretical Physics - Innsbruck, Austria, 1973), pp. B1–B52.
[31] S. Coulibaly, E. Louvergneaux, M. Taki, and L. Brevdo, Eur. Phys. J. D **69**, 186 (2015).
[32] V. E. Zakharov and A. A. Gelash, Phys. Rev. Lett. **111**, 054101 (2013).
[33] B. Kibler, A. Chabchoub, A. A. Gelash, N. Akhmediev, and V. E. Zakharov, Phys. Rev. X **5**, 041026 (2015).
[34] M. Yu and C. J. McKinstrie, Phys. Rev. E **52**, 6826 (1995).
[35] L. Brevdo, Geophys. Astrophys. Fluid Dyn. **40**, 1 (1988).
[36] G. S. Triantafyllou, Phys. Fluids **6**, 164 (1994).